Asymmetric supported dense lanthanum tungstate membranes

V. Gil [* †], J. Gurauskis[†], M.-A. Einarsrud

Department of Materials Science and Engineering, Norwegian University of Science and Technology, NO-7491 Trondheim, Norway

Abstract

In this work, a colloidal processing route for dense asymmetric $La_{28-x}W_{4+x}O_{54+3x/2}$ membranes for hydrogen gas separation applications was established. Dip coating process conditions were optimized to obtain ≈20 μm thick dense layer supported on a porous substrate of the same composition. Surfactants based on electrostearic stabilization were evaluated to obtain stable suspensions in ethanol. The effect of the quantity and type (rice starch and carbon black) of sacrificial pore formers was evaluated for the porous substrates. Based on our results, samples made with 35- 45 vol.% carbon black are the best choice to obtain highly porous supports with the optimum characteristics for the fabrication of asymmetric membranes.

---

[*] - Author to whom correspondence should be addressed: gilh@dtu.dk

[†] - Current address: Department of Energy Conversion and Storage, Technical University of Denmark, Frederiksborgvej 399, 4000 Roskilde, Denmark.

Introduction

Lanthanum tungstates, $La_2O_3:WO_3$ (LWO) with a molar ratio ~3:1, have attracted attention due to their relatively high mixed proton-electron conductivity at high temperatures and good stability in moist CO_2 environment making them an interesting material for dense hydrogen permeable membranes [1-5]. Especially the compositions $La_{28-x}W_{4+x}O_{54+3x/2}$ [6] giving La:W ratios in the range 5.6 to 6 have been carefully studied. La_6WO_{12} exhibits n- and p- type electronic conductivity under reducing and oxidizing atmospheres at high temperatures, respectively, determined from electrical measurements by Haugsrud et al. [3, 4]. In our previous work [5] on hydrogen permeation in asymmetric $La_{28-x}W_{4+x}O_{54+3x/2}$ (x= 1.22, La:W ratio ~ 5.6) membranes it was established that the defect situation is not the same in the whole temperature range up to 1000 ºC e. At 800 − 850 ºC there is a shift, where below that temperature the permeation is limited by n-type conductivity and above by n-type conductivity. Further, adding water vapor enhances the hydrogen permeation at temperatures above 950 ºC [5].

In order to assess the true potential of these materials it is important to measure hydrogen permeation directly on thin supported membranes, as permeation estimates from conductivity data often are based on simplified models and permeation measurements on thick samples can conceal possible surface kinetic limitations [7]. For industrial applications of LWO-based materials, asymmetric membranes are also the preferred geometry to achieve high enough hydrogen permeation. However, works reported on the colloidal fabrication of lanthanum tungstate (LWO thin films are scarce, and it is therefore a need to define the processing route conditions for this novel material. Apart from challenges to maintain desirable LWO stoichiometry, the processing route should be cheap and industrially scalable due to

economical/applicability concerns. Ceramic consolidation routes based on colloidal processing are widely used within the technical ceramic industry and are based on stable ceramic oxide particle suspensions in aqueous or organic media [8].

In this work, asymmetric membranes based on lanthanum tungstate with composition $La_{28-x}W_{4+x}O_{54+3x/2}$ (x= 1.22, La:W ratio= 5.6), hereinafter denoted as LWO56, were fabricated by colloidal processing. A processing route based on dip coating of ~20 μm LWO56 dense membrane on porous LWO56 supports was developed. The quantity and type of sacrificial pore formers such as carbon black and rice starch within porous LWO56 supports was assessed. The deposition of a dense layer by dip coating of a colloidal suspension on highly porous support should address the issue of highly irregular surface topography of the support. The irregular surface is caused by the use of pore formers resulting in holes and defects on the substrate surface that can not be covered efficiently by relatively thin dense functional layer. To smoothen the surface of the porous support and ensure gas tightness of the asymmetric membrane, a porous bond layer between the porous structural support and the dense membrane layer was adapted.

1. Experimental part

1.1. Asymmetric membrane preparation

The lanthanum tungstate powders were synthesized by spray pyrolysis and different heat treatments (700 or 1000 ºC) were done in order to obtain powders with different characteristics. Detailed synthesis procedure was reported previously [9]. Powders with specific surface area of ~ 6 and ~ 9 m^2/g and average particle size, d_{V50} = 900 nm and

400 nm were used as starting materials for the porous support/bond layer and dense layer, respectively.

Porous supports (25 mm diameter, 2 mm thickness) were uniaxially pressed with the addition of pore formers (35-52 vol.%). The LWO56 powder and pore former mixtures were homogenised in ethanol by ball milling for 15 min. Two commercially high purity pore formers with different particle shape, particle/agglomerates sizes and decomposition temperatures were compared: rice starch (DR-LA, REMY industries) and carbon black (charcoal activated, Merck Chemicals KGaA).

Slurries for dip coating of the porous bond layers were prepared in two steps. In the first step, LWO56 powders, carbon black as pore former and polyvinyl butyral (PVB) as the binder were dispersed in ethanol and ball milled for 24 h in order to obtain a homogeneous distribution of the constituents. In the second step (and prior to rheological characterization) the suspensions were slowly rolled (Roller mixer RM10W CAT, Staufen, Germany) for 24 h to age them and eliminate air bubbles. The slurry compositions (Table 1) with varying solid content of ceramic powders, pore former and binder content were evaluated.

Suspensions for dip coating of dense layers (2 vol.% solids) were prepared by ultrasonically dispersing LWO56 powders with varying surfactant content (0.5-3.5 wt.% of LWO56) in pure ethanol. Two electrosteric surfactants were studied: surfactant 1 - polymer with polar groups (Dolacol D 1003, Zschimmer & Schwarz GmbH) and surfactant 2 - short chain polar surfactant (Acetic acid, Sigma Aldrich).

The dense layer deposition (and porous bond layer if needed) was performed by dip coating during 10 s holding time (5 s for porous layer) with immersion and pulling out speeds within the range of 1 to 2 mm s^{-1}. Prior to dip coating the suspensions for the dense layers were diluted to 0.75 vol.% of solid content. After each coating step, the

sample was presintered at 1100 ℃ for 1 h using 2 ℃/min heating and cooling rates. When the porous bond layer was deposited an additional calcination process was carried out; more details about this step are given later. Two coating-presintering cycles were needed to achieve the desirable thickness of the dense membrane layer.

The asymmetric membranes were co-sintered in one step at 1420 ℃ for 3 h in ambient air (2 ℃/min). These conditions ensured suitable characteristics of the LWO56 material for the use as a membrane: single phase, full densification with homogeneous microstructure and no exaggerated grain growth [9].

1.2 Characterization

The decomposition temperature of the pore formers was studied by thermal analysis up to 1000 ℃ in air with a heating rate of 5 ℃/min (STA 449C, Netzsch, Selb, Germany). The morphology of the pore former powders dispersed in ethanol was compared by scanning electron microscopy (SEM, Hitachi S3000N). Particle size distribution was carried out in aqueous media by laser diffraction analyzer (Mastersizer 2000, Malvern Instruments, UK). Porosity of the sintered porous supports was obtained from density measurements by Archimedes method in 2-propanol. SEM images were also used for the estimation of porosity as well as for pore size distribution by image analysis using the high degree of contrast between the dark pores (voids) and highly reflective LWO56 material. Prior to SEM analysis, the samples were vacuum imbedded with a low density resin (Epofix Struers, USA) and cured for 24 h at 60 ℃, followed by polishing with 9, 3 and 1 μm diamond suspension. . Previously, this image analysis method for specific experiments and metallographic conditions was statistically tested to give a 95% confidence level [10].

The effect of the type and quantity of sacrificial pore formers on porosity of LWO56 porous supports was done by estimating the gas permeability coefficient K ($m^2 \cdot s^{-1}$) [11]:

$$J = K \cdot \frac{\Delta p}{l} \tag{1}$$

where J is gas flux ($kg \cdot m^{-2} \cdot s^{-1}$), l is membrane thickness (m) and $\Delta p = p_1 - p_2$ is the pressure difference (bar) across the membrane. If the pore sizes in the porous support are comparable or less than the mean free path of the gas, the flow becomes free molecular (Knudsen or slip-flow regime). This effect can be estimated generally by:

$$K = K_0 + \frac{B_0}{\eta} \cdot \bar{p} \tag{2}$$

where K_0 is the Knudsen permeability coefficient ($m^2 \cdot s^{-1}$), B_0 is specific permeability coefficient (m^2) of porous media, η is the viscosity of the gas ($N \cdot s \cdot m^{-2}$) and $\bar{p} = 0.5(p_1 + p_2)$ is the mean pressure (bar).

The gas permeability of LWO56 sintered porous supports was evaluated at room temperature (293 K) using pellet type geometry samples of ~ 0.1 cm in thickness (l) and surface area (after mounting to apparatus) of 1.1 cm^2. The samples were mounted using soft rubber rings within a tubular chamber leaving one side exposed to air at ambient pressure (p_1) and another side exposed to pressurised (p_2) synthetic air. The uncertainty of the recorded steady state gas flux (J) and pressure (p_2) at the pressurised part of the chamber was of 0.001 $kg \cdot m^{-2} \cdot s^{-1}$ and 0.1 bar, respectively.

Thw zeta potential of LWO56 powders in suspensions with varying type and amount of surfactants was measured using electrokinetic light scattering technique with Zetasizer NS (Malvern Instruments, UK). Standard disposable cells were filled with supernatants

of optimum concentrations for measurement and 15 runs were performed for each composition.

Rheological characterization of the slurries was done with rotational rheometer Mars III (Haake, Karlsruhe, Germany) equipped with double cone-and-plate test geometry (titanium double cone of 1°, $\varnothing$ = 60 mm). Flow curves and corresponding thixotropy of the samples were recorded using controlled share rate (CR) mode at shear range 0.1 - 500 s^{-1} and dwell time of 30 s at maximum shear. Dynamic viscosity was measured at a constant shear rate of 100 s^{-1} taking the average value recorded during 30 s. Amplitude sweep oscillatory testing was done at a fixed frequency of 0.1 Hz. This frequency was chosen to evaluate the behavior of suspensions close to the conditions of suspension at rest [12]. All rheological measurements were carried out at a temperature of 20 $\pm$0.1 °C and precautions were taken to perform measurements on suspensions at rest with fully recovered structure after pre-shearing at 10 s^{-1} for 30 s.

Microstructural characterization of LWO56 asymmetric membrane cross sections was done by scanning electron microscopy (SEM, Hitachi S3000N) on vacuum imbedded low viscosity resin and polished samples.

2. Results

2.1 Preparation of porous supports

Thermal decomposition behaviour of the carbon black and rice starch pore formers is represented in Fig. 1. Mass loss at relatively low temperature is attributed to humidity in the as-received pore formers, therefore the mass loss directly related to the decomposition is only observed above 300 ºC. Although the carbon black oxidation started when the decomposition of the rice starch powders was completed (500 ºC), the process was faster and was completed within a 100 ºC range. Final residual content after

burnout at 1000 ºC was 0.5 wt.% for rice starch and 1.6 wt.% for carbon black. The slower decomposition kinetics of rice starch might be attributed to decomposition or combustion in two steps. A comparison of the characteristics for the two pore formers studied is summarized in Table 2.

Based on these results, the calcination processes for the green supports controlling the burnout stages and heating rates were defined. A first step for two hours were carried out with a rate of 1 ºC/min up to 350 and 550 ºC for rice and carbon black supports, respectively. To obtain enough structural strength for manipulation before the sintering step, the burnout step of pore formers was followed by a pre-sintering step at 925 ºC for rice starch and 1000 ºC for carbon black (dwell 1 h) with heating rate of 2 ºC/min and cooling rate of 5 ºC/min.

The microstructure of supports with similar porosity, ~ 25 vol.%, is compared in Fig. 2a (45 vol.% rice starch) and Fig. 2b (35 vol.% carbon black). The porous supports fabricated with rice starch showed large and relatively small, isolated and spherical pores whereas those obtained with carbon black showed well interconnected and elongated pores. The microstructure of rice starch samples with non-uniformly distributed large pores is probably due to agglomeration of the pore former.

For comparison the morphology of the pore formers is included in Fig. 2. Rice starch powders were characterized as well-defined spherical agglomerates with ≤ 50 μm in size and about 5 μm as primary particle size (Fig. 2c). Carbon black powders with a mixture of long (~150 μm) and short (~40 μm) lamellae are observed (Fig. 2d). Rice starch has a narrower particle size distribution than carbon black, with d_{V50}=7 μm and the presence of agglomerates between 1 and 30 μm. Carbon black powders with a d_{V50}=50 μm presented a bimodal distribution with a relatively large amount of small particles besides the large particles up to 250 μm.

Figs. 3a and b show the pore size distribution profiles of sintered porous supports made with rice starch and carbon black. In good correlation with the shape of the pore formers, the pores in the samples prepared with rice starch were nearly spherical while the samples with carbon black presented elongated pores and therefore both the length and breadth is given. Porous samples prepared from rice starch presented smaller pores on average than the samples prepared with carbon black. Elongated pores up to 100 μm in lenght, which could play a beneficial role for the gas permeability of the support, were present in the carbon black samples.

Figure 4 shows the apparent porosity for the porous supports determined by Archimedes method and by image analysis. The porosity values calculated by Archimedes method were higher than those obtained by image analysis. Uncertainties in the former for highly porous supports and the non-intentioned discard of the smaller pores through the thresholding during the image analysis of the SEM images might be the reason of these discrepancies. Lower values of the apparent porosity were obtained for the supports made with rice starch compared with the carbon black analogues forthe same content of pore former used.

Estimates of the gas permeability coefficient K for synthetic air at ambient temperaturefor the LWO56 porous supports made using different quantities and types of pore former is presented in Fig. 5. As suggested by Altena et al. [13] the given precision (uncertainty in the pressure of synthetic air (p_2) ≈ 0.1 bar) of gas permeability setup is not sufficient to estimate a mean pore radius within the porous support using theoretical calculations. Nevertheless the estimation of gas permeability coefficient K showed to be very useful when comparing porous supports prepared with different pore formers and their quantities. The gas flow through LWO56 porous supports made with rice starch and carbon black with the lowest addition (30 vol.%) showed little variation in gas

permeability with increasing gas pressure difference. This tendency indicates that the gas flow in these supports is predominantly dominated by Knudsen diffusion and the viscous gas flow is quite negligible. In contrast to that, the porous support made with 42 vol.% of carbon black as pore former showed strong dependence with the gas pressure difference. The significant increase in both Knudsen diffusion and specific permeability coefficients indicates highly interconnected porosity with predominant viscous gas flow regime in this support.

2.2 Porous bond layer

The viscoelastic behaviour of the suspensions for the porous bond layers measured by oscillatory tests is shown in Fig. 6. Gel type behaviour (storage modulus is higher at rest than loss modulus, $G´ > G´´$) of varying magnitude ($G´$ values, Table 1) is measured for slurries BL20-1, 2 and 3 with the highest solid contents. The most diluted slurry BL20-4 resulted in liquid type behaviour ($G´ > G´´$) within the applied deformation range (Fig. 6). Determination of the yield point (limit of the linear viscoelastic range) as a shear stress at the limiting deformation was estimated using the loss factor (tan $(\delta)=G´´/G´$) and values are given in Table 1.

Slurry BL20-4 with the absence of the rigid structure formation at rest, was discharged from the further evaluation due to the possibility of phase segregation between the pore former and the LWO56 phase.

For porous bond layers deposited from suspensions with the highest solid loadings, BL20-1 and 2, cracks appeared on the surfaces after calcination at 1100 ºC for 2 h as shows Fig. 7a. Cracks were not observed in porous bond layers deposited from slurry BL20-3 with lower solid loading (Fig. 7b). Deposition using this slurry resulted in bond

layers with thickness of 15 μm after the final sintering step and was selected for further work.

2.3 Dense layer deposition

The effect of type and amount of surfactant on the zeta potential of the LWO56 powders in ethanol suspensions is shown in Fig. 8. The zeta potential of the LWO56 particles decreased (or the absolute value increased) with the amount of surfactants up to 1.5 wt.%. For higher concentrations of the surfactants the zeta potential was almost constant. The absolute value of the zeta potential was strongly dependent of the surfactant nature. Suspensions with surfactant 2 (acetic acid) presented higher zeta potential (lower absolute value) of the LWO56 particles compared to surfactant 1 (Dolacol D 1003), therefore surfactant 1 was selected for further work.

Independently of the concentration of surfactant 1 (0.5-3.5 wt.% of LWO56 powder), all the suspensions showed pseudoplastic flow behavior with the formation of positive hysteresis (thixotropy) loop. The comparative thixotropy values with dynamic viscosity values at fixed shear rate $\gamma=100$ s^{-1} of LWO56 suspensions withsurfactant 1 within the range from 2 to 3 wt.% are shown in Fig. 9. The dynamic viscosity decreased with increasing surfactant content up to 2.25 wt.%, then the further increase in surfactant content resulted in a steep increase in the dynamic viscosity. Similar trend was observed from thixotropy values, where the lowest value wasobtained for the suspensions with 2.25 wt.% of surfactant 1.

2.4 Asymmetric membrane

Based on SEM images and permeability values, supports with 35 and 45 vol.% carbon black were chosen as suitable as porous substrates in the asymmetric membrane system.

Asymmetric membranes with two different designs were fabricated. LWO56-A denotes asymmetric membranes consisting of a ~1 mm thick porous support with 35 vol.% carbon black and a ~25 μm dense functional layer. LWO56-B denotes asymmetric membrane consisting of a ~1 mm thick support with 45 vol.% carbon black, a ~15 μm thick porous bond layer (from BL20-3 suspension) and a ~25 μm dense functional layer.

Due to a better homogeneity of the pore former in the support with the lowest carbon black content (35 vol.% carbon black), defects on the surface of the calcined porous supports that could result in inhomogeneous deposition/pinholes of the dense membrane were not observed. Therefore the deposition of the dense layer directly on the calcined porous supports was possible.

Fig. 10 shows SEM micrographs of cross sections of polished asymmetric membranes fabricated with and without the porous bond layer. Fully dense ~25-30 μm thick membranes of LWO56 were successfully achieved using both designs. The~15 μm thick porous bond layer in the LWO56-B membrane had a fine and well-interconnected porosity. The porosity of the porous supports of the LWO56-A and LWO56-B asymmetric membranes was in the range 25 and 40 vol.% measured on sintered porous supports without dense layers.

3. Discussion

3.1. Porous bond layer

In order to obtain defect-free and homogeneous porous bond layers by dip coating it is essential to control the rheological parameters of the slurries. Gel type behaviour with rigid structure formation at low deformation levels is beneficial to preserve the homogeneity of the colloidal suspension. This is even more critical when the colloidal

suspension is composed of solid phase constituents with varying density and granulometry like pore former and ceramic material. Due to this (Table 1) the slurry BL20-4 was discharged from further evaluation. Furthermore, the rigid gel structure with the yield point in combination with a fast evaporating solvent prevents the as-deposited layer from sagging, making the dip coating technique applicable for large surface areas.

However, too strong gel type structure (G´) may lead to a lower compaction of the as-deposited layer and result in increased shrinkage upon drying. The increased shrinkage can cause the formation of cracks upon drying or even during further processing steps related to uneven green compact dimensional changes such as pre-sintering or sintering. Reducing the solid loading can easily reduce the structure strength and the yield point (Fig. 6b, Table 1) of the suspensions, but wetting and adhesion properties of the suspensions may become poor leading to peeling problems. This again can be corrected by increasing the binder loading, but that in consequence may alter the rheological behaviour of the suspensions leading to increased structure strength and the yield point values.

During the dip coating (immersion and extraction) in regions nearby the porous support the slurry is subjected to deformation at shear rates of $\sim$1-100 s^{-1} [12, 14]. Pronounced gel type behavior with a strong rigid structure at rest corresponding to slurry BL20-1 led to the deposition of thick and very low green density layer. Similar results were obtained for slurry BL20-2. The deposition of slurry BL20-3 on the porous support, however resulted in a thin and defect free layer after final thermal treatment cycle. This indicates a better solid phase arrangement of BL20-3 slurry after deposition and sufficient green density to avoid cracking during drying.

3.3. Dense layer deposition

In order to achieve high green density of oxide particles, and consequent efficient densification upon sintering, the selection of appropriate type and optimum quantity of surfactant is essential. At too low surfactant content, the amount of additive is not enough to cover the particle surfaces and particles in the suspension tend to form hard agglomerates. In case of the surfactant excess with respect to surface coverage, the interaction between particles in the suspension and free surfactant can promote coagulation and the formation of soft agglomerates [15]. Whenever the agglomeration is present it leads to poorer compaction and thus lower final density of the dense layer. The optimum content of surfactant is dependent on the composition, particle size and morphology of the particles and on the media where the particles will be dispersed.

The two surfactants evaluated in this study posses surface charge and varying length of the polymeric chains, which can activate steric repulsion mechanisms between LWO56 powders in low polar media. From the zeta potential measurements (Fig. 8) it is obvious that even in a solvent with relatively low polarity such as ethanol, both surfactants generate surface charge. Surfactant 2 gave a lower surface charge compared to surfactant 1 and taking into account that it has a short chain it was discharged from further evaluation.

The effect of insufficient coverage or excess of surfactant 1 is clearly observed from Fig. 9. Viscosity and thixotropy values are at its minimum when the optimum amount (2.25 wt.% of solid loading) is used, indicating the lowest interaction between solid phase particles present in the colloidal suspension. Hence the optimum amount of surfactant 1 for the stabilization of the LWO56 particles in order to decrease the presence of the microstructural defects and increase in the green state density is 2.25 wt.%.

The processing conditions defined in this work have been proven in the fabrication of several membranes for hydrogen flux testing. The hydrogen permeation through the membranes was successfully measured with values as high as $0.14 \text{ mL} \cdot \text{min-1} \cdot \text{cm}^{-2}$ at 1000 ℃ (10 vol.% H_2 and 2.5 vol% H_2O) [5].

3. Conclusions

A detailed procedure for the colloidal fabrication of asymmetric membranes based on $La_{28-x}W_{4+x}O_{54+3x/2}$ has been developed. Dolacol D 1003 (2.25 wt.% of solid loading) is established as the optimum type and amount of surfactant for the preparation of LWO56 slurries (considering the concentration range under study). Using a low content of carbon black (35 vol.%) as pore former, the dense functional layer could be deposited directly onto the porous support. one the other hand a porous bond layer resulting in a smooth and homogeneous interface between the porous support and dense functional membrane layer was necessary when a high volume of carbon black (45 vol.%) was used as pore former in the porous support. Both designs led to gas tight asymmetric membranes and the use of carbon black was the best pore former in order to get highly porous and permeable supports for the asymmetric dense membranes, for hydrogen permeation under different reducing conditions. A further work on the successful hydrogen flux testing of these membranes has been reported in previous publication [5].

Acknowledgement

References:

1. Yoshimura, M. and J.F. Baumard, *ELECTRICAL-CONDUCTIVITY OF SOLID-SOLUTIONS IN SYSTEM CEO2-LA6WO12.* Materials Research Bulletin, 1975. **10**(9): p. 983-988.
2. Shimura, T., S. Fujimoto, and H. Iwahara, *Proton conduction in non-perovskite-type oxides at elevated temperatures.* Solid State Ionics, 2001. **143**(1): p. 117-123.
3. Haugsrud, R., *Defects and transport properties in Ln(6)WO(12) (Ln = La, Nd, Gd, Er).* Solid State Ionics, 2007. **178**(7-10): p. 555-560.
4. Haugsrud, R. and C. Kjolseth, *Effects of protons and acceptor substitution on the electrical conductivity of La6WO12.* Journal of Physics and Chemistry of Solids, 2008. **69**(7): p. 1758-1765.
5. Gil, V., et al., *Hydrogen permeation in asymmetric La28-xW4+xO54+3x/2 membranes.* International Journal of Hydrogen Energy, 2013. **38**(7): p. 3087-3091.
6. Erdal, S., et al., *Defect structure and its nomenclature for mixed conducting lanthanum tungstates La28-xW4+xO54+3x/2.* International Journal of Hydrogen Energy, 2012. **37**(9): p. 8051-8055.
7. Bouwmeester, H.J.M., H. Kruidhof, and A.J. Burggraaf, *IMPORTANCE OF THE SURFACE EXCHANGE KINETICS AS RATE-LIMITING STEP IN OXYGEN PERMEATION THROUGH MIXED-CONDUCTING OXIDES.* Solid State Ionics, 1994. **72**: p. 185-194.
8. Reed, J.R., *Principles of Ceramic Processing.* 2nd Edition ed. 1995: Wiley-Interscience.
9. Gil, V., et al., *La28-xW4+xO54+3x/2 Powders Prepared by Spray Pyrolysis.* Journal of the American Ceramic Society, 2012. **95**(11): p. 3403-3407.
10. Fowler, D.B., W. Riggs, and J.C. Russ, *INSPECTING THERMALLY SPRAYED COATINGS.* Advanced Materials & Processes, 1990. **138**(5): p. 41-&.
11. Carman, P.C., *Flow of Gases Through Porous Media.* 1956: Academic Press.
12. Mezger, T.G., *The Rheology Handbook: For Users of Rotational and Oscillatory Rheometers.* 2006: Vincentz Network.
13. Altena, F.W., et al., *SOME COMMENTS ON THE APPLICABILITY OF GAS PERMEATION METHODS TO CHARACTERIZE POROUS MEMBRANES BASED ON IMPROVED EXPERIMENTAL ACCURACY AND DATA HANDLING.* Journal of Membrane Science, 1983. **12**(3): p. 313-322.
14. Barnes, H.A., *A handbook of elementary rheology.* 2000: University of Wales, Institute of Non-Newtonian Fluid Mechanics.
15. Rosen, M.J., *Surfactants and Interfacial Phenomena.* 2004: Wiley.

Tables

Table 1. Compositions of slurries used for dip coating of the porous LWO56 bond layer and their viscoelastic parameters.

Slurry code	Carbon black (wt.% of LWO56 powder)	PVB (wt.% of total solid load)	LWO56 (vol.%)	Solid content (vol.%)	Rheological parameters		
					Storage modulus G' (mPa)	Flow point τ_f (mPa)	Yield point τ_y (mPa)
BL20-1			4.5	7.4	892	78.5	26.9
BL20-2	20	2	2.25	3.7	857	14.4	3.4
BL20-3			1.97	3.24	239	11.1	2.9
BL20-4			1.78	2.74	--	--	--

Table 2. Characteristics of rice starch and carbon black powders used as pore formers.

	d_{50} (μm)	Powder morphology	T burnout (ºC)	Residuals at 1000 ºC (wt.%)
Rice starch	7	round agglomerates	300-500	0.5
Carbon black	50	lamellae	500-600	1.6
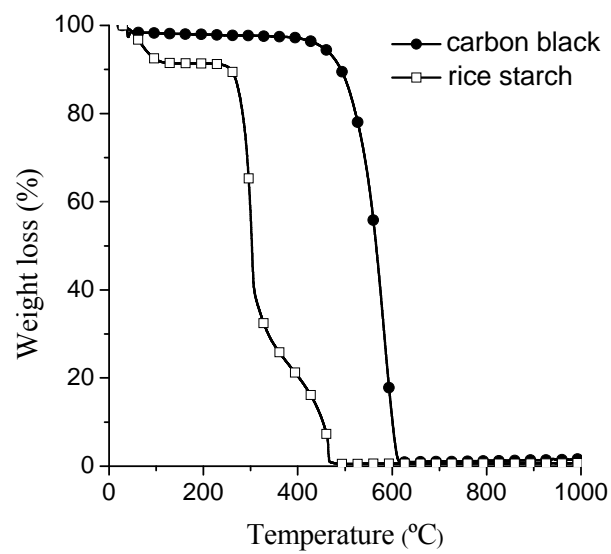
Figure 1. Thermogravimetrical analysis of pore formers carried out in air from RT up to 1000 ºC at 5 ºC/min heating rate.
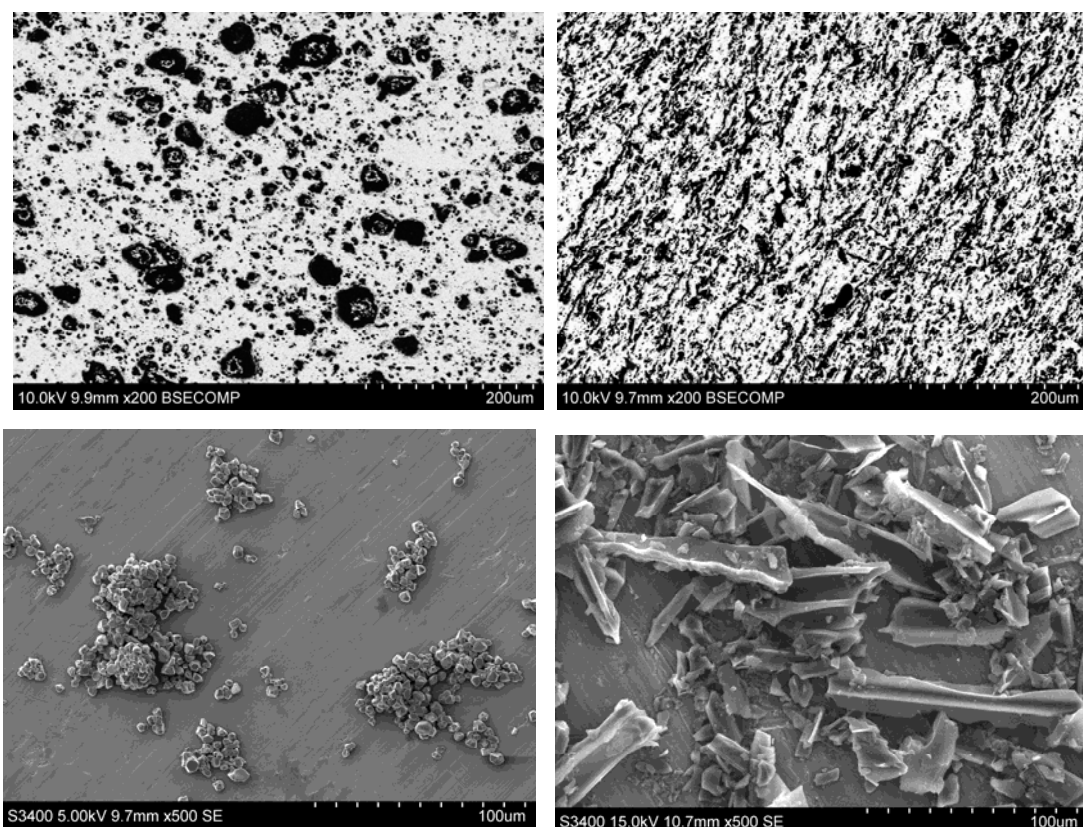
Figure 2. SEM micrographs used for image analysis of sintered LWO56 porous supports made from (a) 45 vol.% rice starch and (b) 35 vol.% carbon black. SEM micrographs of pore formers: (c) rice starch and (d) carbon black.
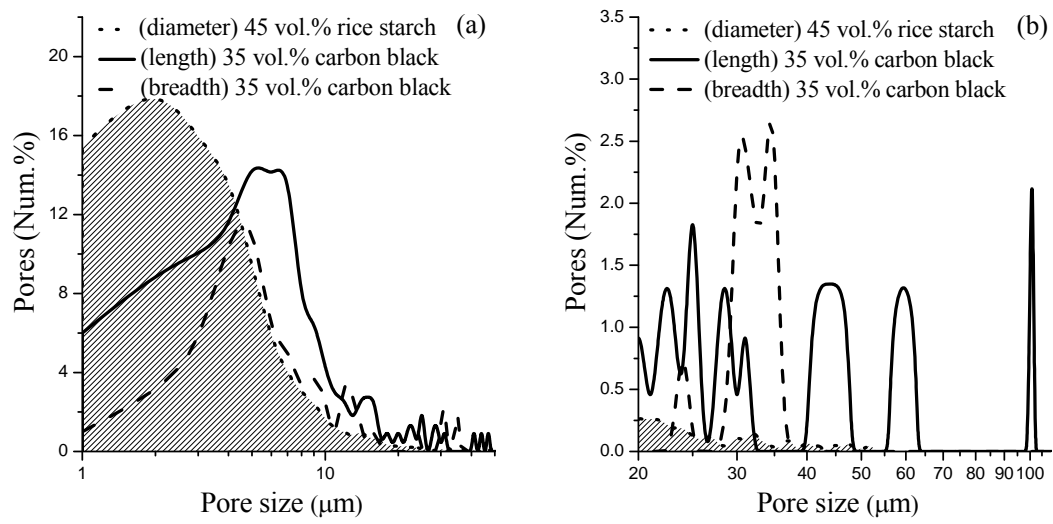
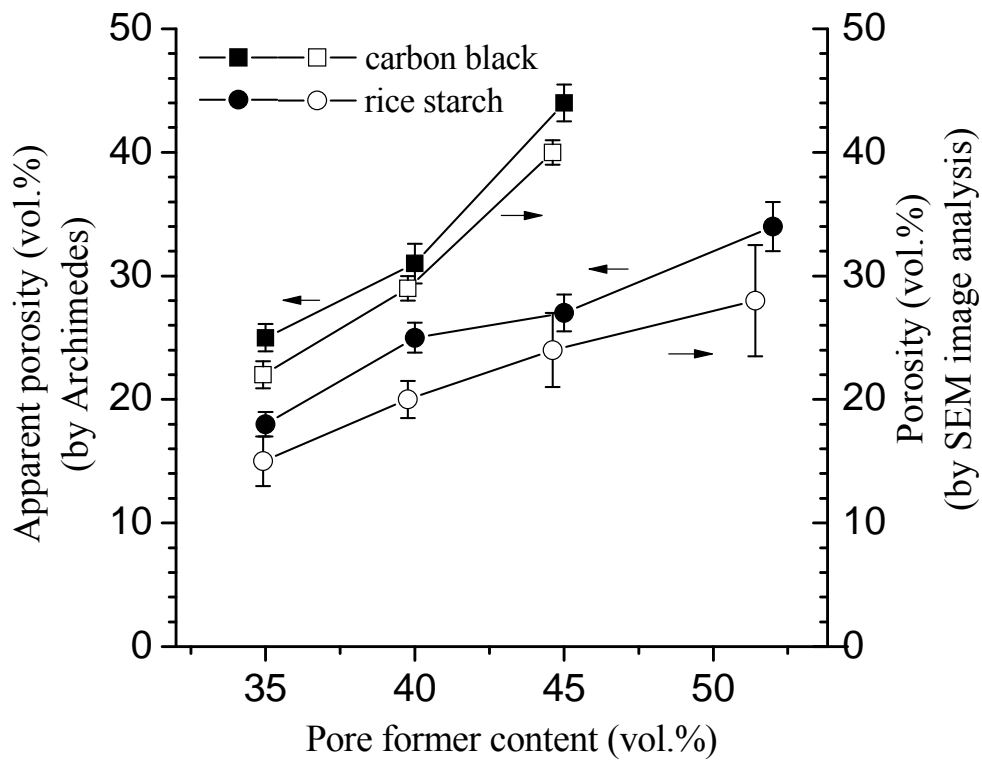**Figure 3.** (a) and (b) Pore size distribution measured by image analysis of sintered porous supports.

Figure 4. Effect of the pore former content and type on the vol.% of porosity generated in the LWO56 porous supports. Measured apparent porosity from Achimedes' method is compared with porosity vol.% obtained by image analysis.
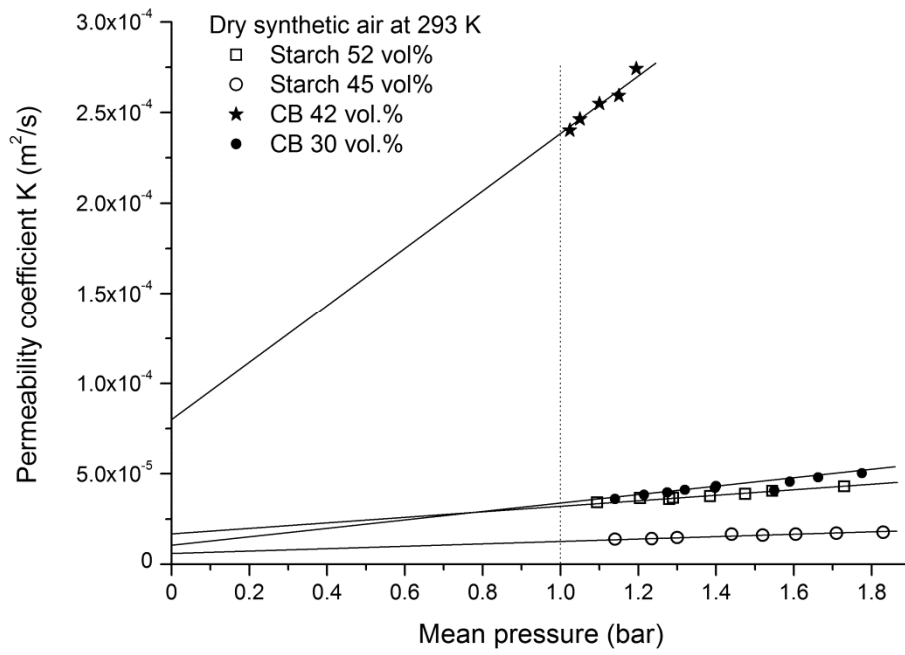
Figure 5. Gas permeability coefficient, K, for synthetic air as a function of mean pressure obtained for LWO56 porous supports made using different quantities and types of pore former.
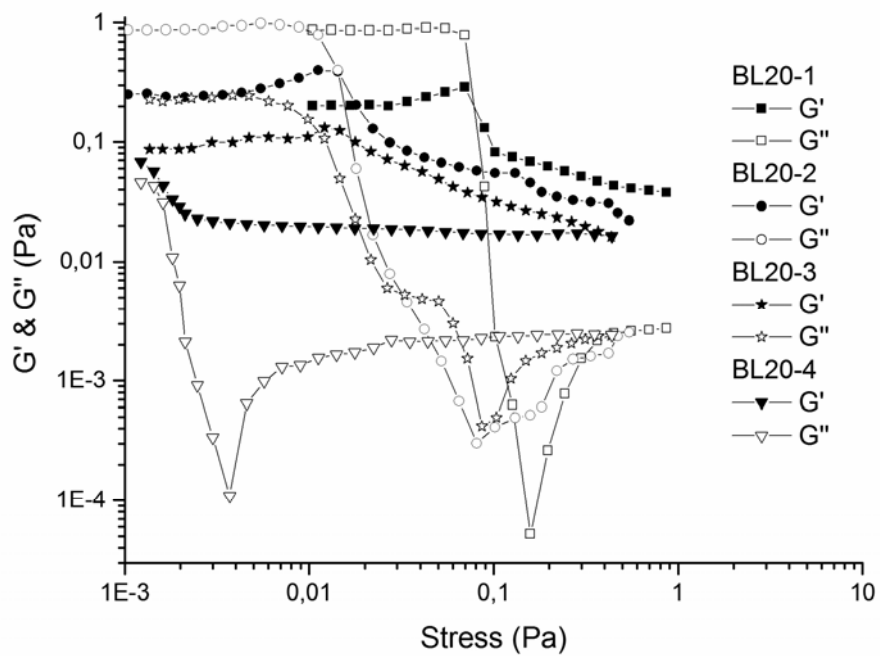
Figure 6. Viscoelatic properties of bond layer slurries recorded at a fixed oscillation frequency of 0.1 Hz.
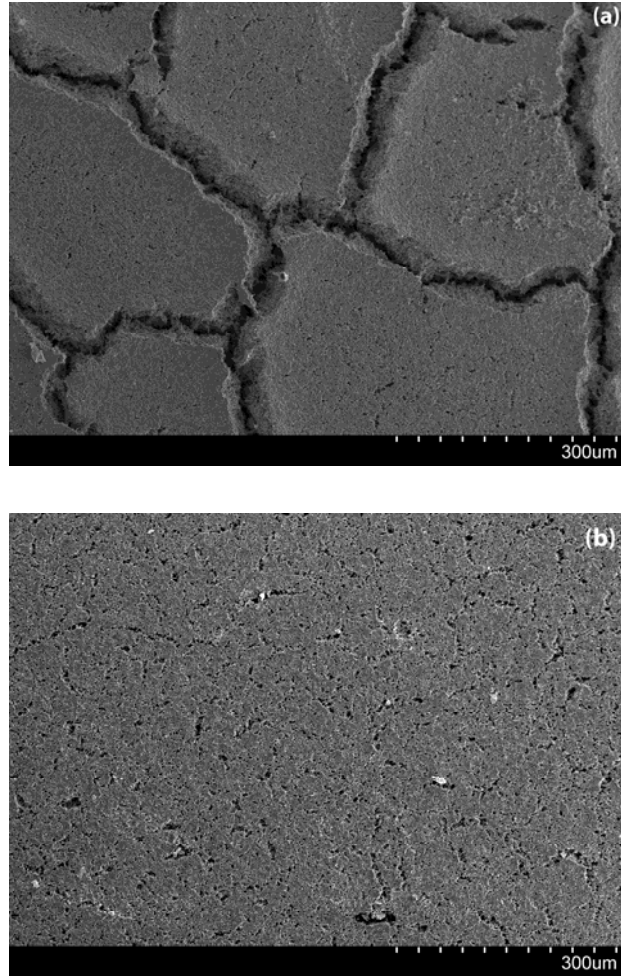
Figure 7. SEM micrographs of the top views of LWO56 porous bond layers coated on porous substrates after calcining at 1100 ºC for 2 h. (a) BL20-1 and (b) BL20-3.
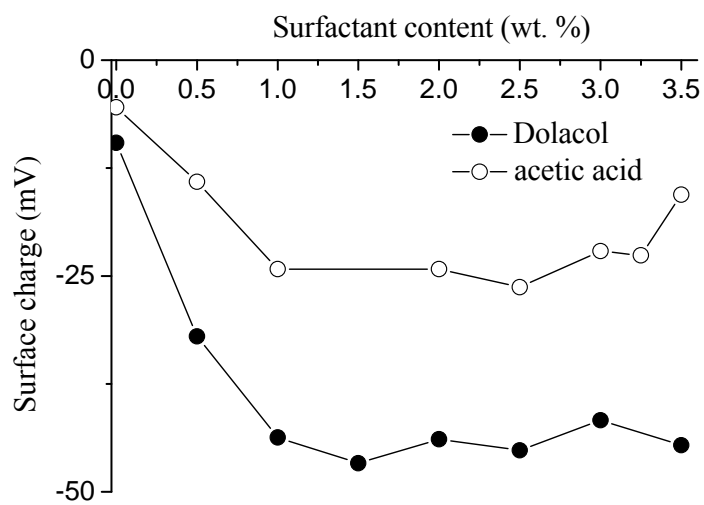
Figure 8. Zeta potential of LWO56 powders in ethanol as a function of type and content of surfactant.

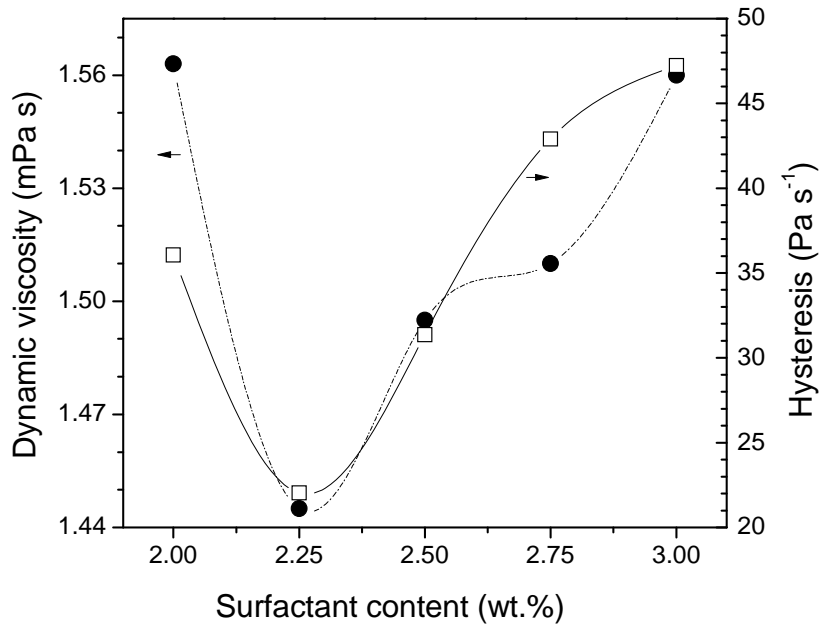Please change label on y-axis to be "Zeta potential" and along x-axis to be "Surfactant content (wt.%)"

Figure 9. Viscosity ($\gamma=100$ s^{-1}) and hysteresis loop ($\gamma=0.1$ - 500 s^{-1}, dwell 30 s at γ_{max}) values for ethanol suspensions of LWO56 as a function of surfactant 1 content (Dolacol).
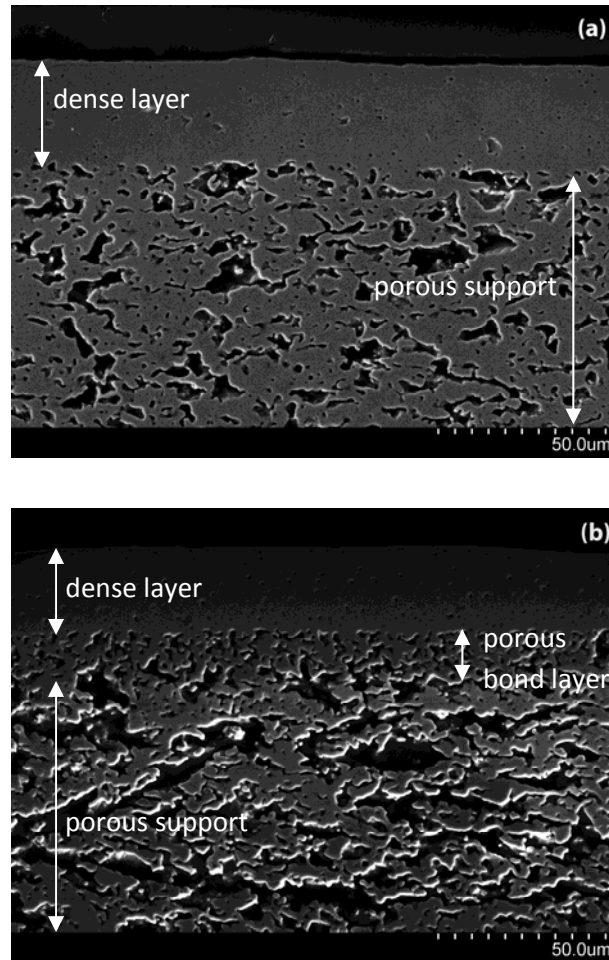
Figure 10. SEM micrographs of polished cross sections of sintered asymmetric membranes (a) LWO56-A, 30 μm thick membrane supported on 25 vol.% porosity substrate and (b) LWO56-B, 25 μm thick membrane supported on 40 vol.% porosity substrate with 15 μm porous bond layer.